Seasonal impact-based mapping of compound hazards

*Hillier, J.K. [1] and Dixon, R. S. [2]

[1] *Geography, Loughborough University, LE11 3TU, UK.*

[2] *Dept. of Meteorology, University of Reading, RG6 6BG, UK.*

**Corresponding Author: j.hillier@lboro.ac.uk*

This paper is a non-peer reviewed preprint submitted to *Env. Res. Lett.* June 15th 2020

Key words: Compound hazard, flooding, wind damage, extratropical cyclone, storm

Impact-based, seasonal mapping of compound hazards is proposed. It is pragmatic, identifies phenomena to drive the research agenda, produces outputs relevant to stakeholders, and could be applied to many hazards globally. Illustratively, flooding and wind damage can co-occur, worsening their joint impact, yet where wet and windy seasons combine has not yet been systematically mapped. Here, seasonal proxies for wintertime flooding and wind damage are used to map, at 1x1° resolution, the association between these perils across Europe within 600 years as realized in SEAS5 hindcast data. Paired areas of enhanced-suppressed correlation are identified (Scotland, Norway), and are shown to be created by orographically-enhanced rainfall (or shelter) from prevailing westerly storms.

1. Introduction

Considering hazards in isolation may both over- and under-estimate risk (1–4), and ‘compound risk’ is emerging as a term to encompass research to identify and understand the impact of combined hazards (5). Over meteorological timescales (hours to weeks), even the joint behaviours of hazards whose origin involves notably different physical processes (e.g. damaging wind, extreme cold or heat, fluvial flooding, storm surge) is widely studied (6–12). Over climatological timescales (seasonal to annual), often invoking a climate mode such as the North Atlantic Oscillation (NAO), there are multi-hazard reviews (13), but a focus has been on individual hazards (14–17) or pairwise extremes of a single variable such as temperature (hot/cold) or precipitation (wet/dry) (18,19). Links between potentially time-lagged events of different hazard types via persistent underlying environmental conditions (2,20) are less studied, especially when also adopting an impact-centric approach. Using flooding and wind damage in Europe as an example, we illustrate that impact-based mapping can identify scientifically interesting phenomena using measures of aggregated risk over a planning timescale of interest to infrastructure operators, government agencies, and (re)insurance.

Flooding and wind damage are two of Europe's most impactful hazards (21). They are commonly assessed separately (14,22,23) although, at meteorological timescales, case studies of strong storms (low-pressure systems, extratropical cyclones) show both classes of damage can co-occur during the same weather system (24–28). Intriguingly, when only short timescales (<72 h) are used to map precipitation-wind correlation across Europe (12), the dependency is weak in Great Britain (GB). In contrast, a substantive correlation for the GB is proposed to exist ($r_p \approx$ 0.4-0.7, p < 0.05) in longer time-windows (2,4,11,29). A way to reconcile these observations is the proposal of Hillier et al. (2) that compound risk is elevated by a systematic, multi-storm relationship on timescales up to seasonal (hours to months), driven by persistent underlying environmental conditions. It has not yet been possible to fully assess this idea as the GB estimates represent a single national figure (2,11), short time-series (~15 years, Hillier *et al* (2,4)), or climatic variables that are not established to be metrics relating to impact (e.g. 29,30). Thus, to overcome these limitations, we advocate using seasonal-scale proxies for damage to map where flooding and wind impacts do or do not compound across Europe.

2. Method & Data

Investigations of compound risk (2,29,31,32) select appropriate proxies for impact (Fig. 1). Here, the hypothesis is that flooding and extreme wind are linked by persistent underlying environmental conditions (2,4), so hazard proxies at a seasonal timescale are selected (dashed outline). Over a season stochastic, sporadically occurring and relatively uncommon extremes accumulate, permitting any coherent 'signal' of correlation to be detected most readily. Any sub-seasonal time-lags between events (11) are implicitly accounted for. Hazard proxies are based on weather/climate metrics, but calibrated to loss data, avoiding the limitations of loss data (e.g. spatially sparse, short term) whilst being 'impact-based' in that they are designed to relate to loss (e.g. 33) .

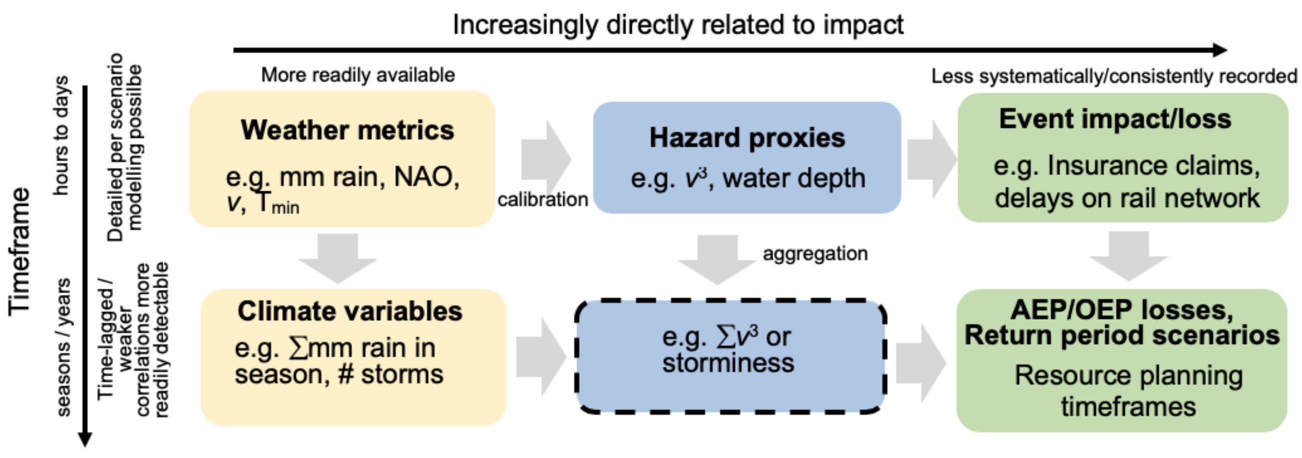

Fig. 1 - Two-dimensional typology of proxies for the impact of natural hazards. In how directly they are related to impact, x-axis, proxies range from climatic variables (e.g. mm/yr), to hazard proxies (e.g. v^3), to quantifications of particular classes of damage (e.g. insurance losses). Proxies may cover short or long durations, y-axis. Seasonal-scale, impact-based hazard proxies are advocated here (blue box with dashed outline).

The seasonally aggregated proxies used are $D_R = \sum R$ for flooding, and $D_W = \sum(v_{max} - c)^3$ for $v_{max} > c$ for wind damage. *R* is total daily precipitation in mm, v_{max} is daily max 10-m gust wind speed, and *c* is a threshold over which damage is thought to occur. Whilst a percentile might be taken for *c* (34), 20 ms^{-1} is taken as damage to buildings increases markedly and non-linearly above this (35,36). v^3 is used as total power dissipation in wind storms, the energy available to do damage, rises roughly as v^3 (15,33,37,38). Aggregated winter precipitation is proposed for D_R on the two-fold basis that antecedence (e.g. via soil saturation) is important for precipitation-driven hazards (11,39,40), and D_R observations in the period 2006-2019 correlate with losses from delays on the rail network of Great Britain (GB, r_p^2 = 0.63, *p* = 0.0012, Fig. S1). Sensitivity tests to the functional form of D_R and choice of *c* and are in Supp. Matt. sections SM1 and SM2.

v_{max} and *R* data are from SEAS5, the ECMWF Seasonal forecast System 5, re-gridded to 1°x1° (41,42). Each member of the SEAS ensemble (versions 4 or 5) is a physically consistent realisation of a potential reality (43,44). SEAS5 hindcasts have 25 members spanning 24 years (1993-2016) considered by ECMWF to be most relevant to the current day in the context of climate change (45). Simulations run for 7 months, and September re-forecasts are chosen to capture the 'winter' half-year (Oct-Mar) when it is assumed the imprint of initialization conditions will have faded and the ensemble diverged sufficiently (44). Namely, September itself is excluded to remove 'real' weather. This approach (43,44,46–49), as used here, gives 600 simulated years (24 years × 25 members) that might plausibly have occurred.

Compounding is mapped (Fig. 2d) by an uplift (U) in mean wind damage (D_W) in the wettest one third as opposed to the driest one third of years; namely, a fraction (f = 0.333) of years are taken as wet. The statistical significance of U is determined by a t-test. Correlations, Pearson's (r_p) and Spearman's rank (r_s), between D_W and D_R are examined to support this at selected sites (Figs. 2a-c, S2). To understand impact, exceedance probability (EP) curves are plotted (Figs. 2g-i), with statistical significance determined by a stochastic simulation (10,000 iterations) to detect differences from an uncorrelated state (2,50–52). The procedure to calculate aggregate EP (AEP) curves is standard (21). Whilst noting advances in statistical modelling multivariate extremes (6,52–56), to make the approach as accessible as possible we select the simplest sufficient methods.

3. Impact-based map of compounding hazards

To build upon the studies of Great Britain (GB), and mapping in short time windows (24-72h), impact-based proxies for flooding (D_R) and wind damage (D_W) are used to map how these perils compound across Europe on a seasonal timescale (Fig. 2d). In the Atlantic to the north and west of GB, there is an uplift of roughly +100% wind damage potential in wet years (pink). This background level of correlation (Central site C, Fig. 2c) is modified across the north of GB, enhanced to the west (Western site W, Fig. 2a) and suppressed to the east (Eastern site E, Fig. 2b). Similar patterns of enhanced-suppressed correlation occur across Scandinavia (Norway/Sweden) and the Iberian Peninsula. Elsewhere, the background level of correlation is maintained across northwest central countries (France, Germany), whilst low and statistically insignificant effects (white/blue colours, circles) are present over southern areas (e.g. Italy). This spatial pattern (relative magnitudes) is broadly insensitive to the measure of correlation used (U, r_p, r_s), threshold c, fraction f of years defined as 'wet' or 'dry', or indeed a shorter Nov-Feb winter (Fig. S2). In terms of wider implications, the map demonstrates that using impact-based seasonal proxies is a pragmatic means of mapping compounding hazards. In detail, we acknowledge that local (sub-grid) associations and variations are not captured, perhaps exposed hilltops outside mountainous areas (e.g. SW England) or between neighbouring valleys (57), and that some mechanisms for flooding such as snow melt (e.g. 40) may not be fully accounted for.

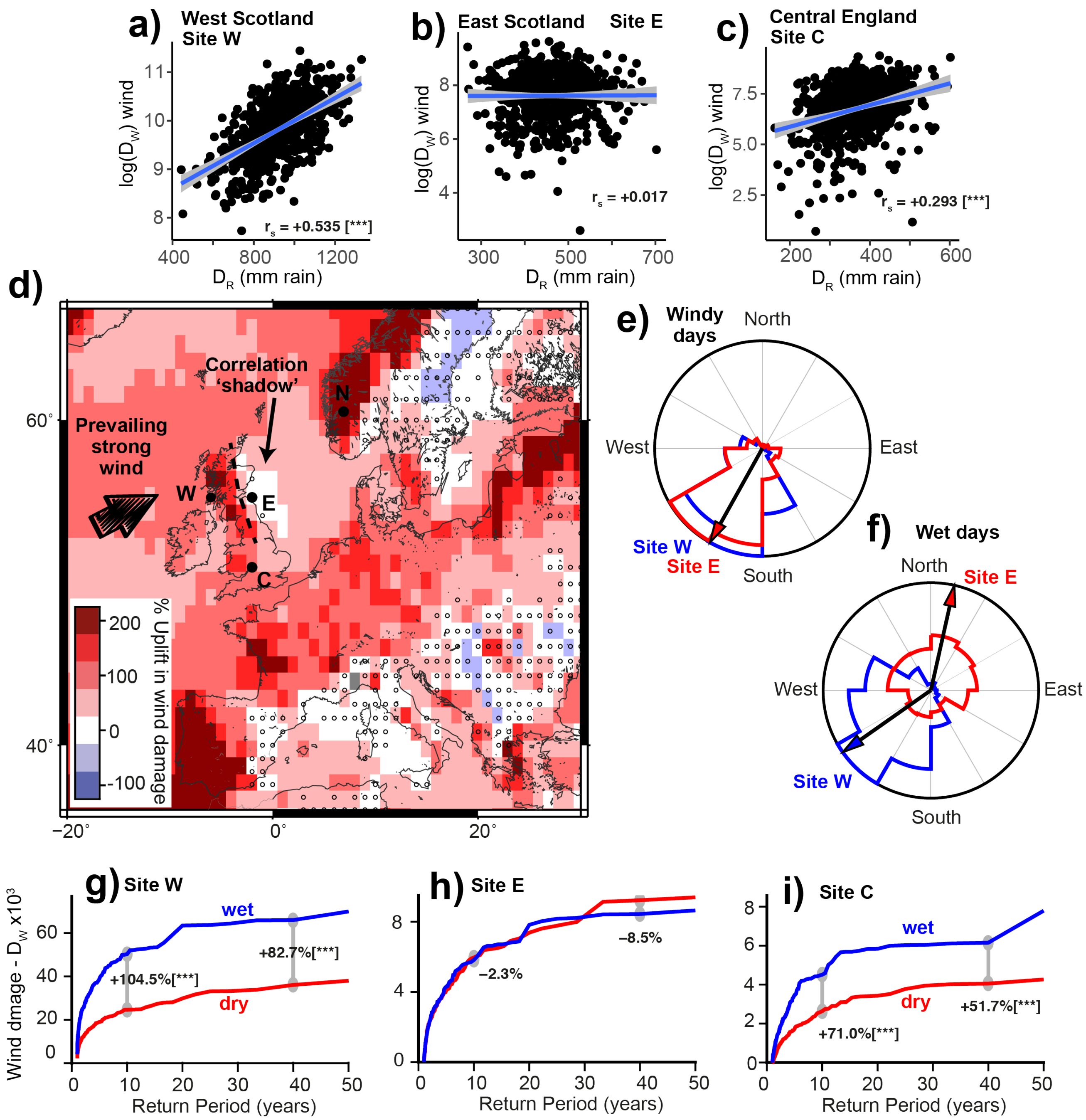

Fig 2 - Impact-based estimate of compounding between flooding and extreme wind (a) - (c) Scatter plots of the seasonal hazard proxies D_R and D_W, with OLS best-fit lines and 3σ confidence intervals, at sites W/E/C located in panel d. (d) Map of uplift $U = 100 * (D_{w\_wet}/D_{w\_dry} - 1)$ in wet over dry years with *f*=0.33. Circles indicate a lack of statistical significance. (e) Orientation of winds on windy (>99th percentile) days for sites W and E. (f) as panel e but for wet days. (g) - (i) AEP curves for D_W, for wet (blue) and dry (red) seasons at the three sites. Differences given at 10 and 40 year return periods. Where statistically significant, p values are in []; * <0.1, ** <0.05, *** <0.01. Site locations: W (-006°,56°), E (-002°,56°), C (-002°,52°), N(001°,61°).

4. Enhanced compounding and correlation shadows

Fig. 2d presents a view of the potential for flooding and wind damage to combine at seasonal timescales. The areas of strongest co-occurrence when only short (≤72h) timeframes are considered (12), in North and Baltic Seas, are muted leaving paired areas of enhanced-supressed risk (Norway, Iberia, GB, South Sweden, South Italy) more distinct. Statistical simulation modelling (Supp. Matt. section SM5) provides an explanation for the increased clarity, with the majority of the compounding effect (~70-90%) at sites W/C/N attributable to a relationship at timescales over 72h. A striking difference between Fig. 2d and mapping of short-term correlation (12) is GB. We therefore choose to investigate the patterns and mechanisms here in more depth and detail than done previously.

Flooding and wind damage proxies in Great Britain compound most strongly in the north, to the west of the hills that run northwards from the Pennines into the Scottish Highlands (Fig. 2d). Storms and strong winds predominantly hit GB from the south-west (Fig. 2d)(14,24,58). In these low-pressure frontal systems, the heaviest topographically enhanced rainfall occurs in the warm sector of the depressions in association with strong winds (59–61). This orographic enhancement over this moderate amplitude topography is widely thought to be caused by the seeder-feeder mechanism (61–63), and the rainfall is the main driver of flooding in affected areas (e.g. 64–66). In SEAS5, these behaviours are evident in the agreement of wind directions for the windiest and wettest days at Site W (Fig 2e-f, blue), and the correlation between daily wind and rain (v_{max} and *R*) at site W is high (r_s= 0.607, *p* < 0.01) matching that of the seasonal proxies (Fig. 2a). However, this is not a complete explanation as the very windiest days are wet but not the wettest ones (Fig. S3). We suggest that this is because storms with the most damaging winds are likely to still be actively interacting with the jet stream and therefore intensifying and travelling rapidly (67,68), allowing them less time than slower-moving systems to rain at any given site on the ground; their translational speed likely adds only a minor amount to v_{max} (21,69). Therefore, persistence appears to also play a role in creating the enhanced correlations in Fig. 2, either from clusters of storms within relatively short time windows ($\lesssim$14 days) to create widespread flooding (11,23,70) and/or on climatological timescales (weeks/months) to create notably wet and stormy winters (4,29,32,71–73).

East of the hills, correlation is suppressed, to which we give the label 'correlation shadow' (Fig. 2b). This decorrelation arises because winds bearing the most intense rain to site E (northerly) come from a different direction to the strongest winds, which are from the south-west and not the north (Fig. 2 e-f)(58). Daily v_{max} values show that the strength of the severest gusts at the sites is strongly related (r_s= 0.773, *p* < 0.01), indicating that both typically arise from the same weather patterns, but extreme rain does not commonly follow at site E. This can be partially understood by the concept of a rain-shadow (12,74,75). This is not as unambiguously invoked in GB as it is for larger mountains (76), but the strongest rain-shadow effect occurs for precipitation in the warm sector of frontal systems (77,78) like those driving the compounding effect at site W.

What rain persists eastwards, might still produce risk correlated with wind, but is does not as its direction is not consistent with the wettest days at site E (Fig. 2f). Thus, the key to understanding Fig. 2d is the difference in site-specific response to a similar set (Fig. S4) of impacting weather patterns or air masses. At a seasonal level, wind directions (weather types) capable of causing flooding and wind damage in GB are known to trade-off with each other (79–81). In particular, when westerly winds are common those from the north and east occur less frequently (Fig. S5), but this effect does not appear strong enough to induce inverse relationships (Fig. 2d,h) as none are statistically significant.

This example highlights that using seasonal hazard-based proxies can identify phenomena to investigate further (e.g. with daily data), and poses questions to drive future research. How does the mechanism driving GB's correlation shadow compare to that of Scandinavia or the western USA? How prevalent is each type of extra-tropical correlation shadow globally? How strong is compounding in the most extreme seasons/events? How will these change in future?

5. Impact of compounding effects

Many stakeholders, such as the (re)insurance sector or rail network, need to understand rare and extreme years for the purposes of planning. Will the compound aggregate loss in a season likely exceed their limits permitted by regulation, capacity or reserves? A correlation driven by small but frequent losses is not a concern, whereas one that exhibits itself as both very severe flooding and wind damage in the same year would be. Therefore, with wet years linked to increased flooding impacts (Fig. S1), an important result (Figs 2g,2i) is that the flood-wind correlation identified from relatively short time series (2,4,11,12,29) is securely established present at higher return periods up to ~50 years from 600 years of data. Thus, the use of seasonal, impact-based hazard metrics has allowed us to build additional understanding of real-world relevance over and above that possible from the relatively short instrumental record.

6. Conclusions

By applying seasonal, impact-based hazard proxies to map how flooding and extreme wind compound across Europe, using SEAS5 data, our view is that such mapping is useful for three main reasons:

1. It is a pragmatic, self-consistent (i.e. using similar data) means to map compounding hazards across large regions using publicly available data (e.g. SEAS5). This said, where possible we advocate site-specific studies using alternative data (e.g. river flows, weather station data) and higher resolutions (spatial and temporal) to validate the observations and gain deeper process-based understanding (e.g. 82).
2. The mapping identifies phenomena (e.g. correlation shadows) to drive the research agenda, posing questions and generating hypotheses about atmospheric behaviour for future investigation and testing.
3. The outputs (e.g. % increase in losses, AEP curves) are seasonal, at a time-scale relevant to many stakeholder's resource planning horizons, and thus of direct real-world relevance.

This approach could readily be applied to different regions, or to diverse and potentially time-lagged hazard combinations (e.g. landslide, snow, heat, wind).

Acknowledgements

We thank Rob Wilby and Alex Alabaster for their comments, which improved this work. Hillier is funded by the UKRI, NERC KE Fellowship NE/R003297/1.

Author Contributions Dixon conceived the work. Hillier and Dixon together devised and conducted the analyses, reviewed existing literature, discussed the results and wrote the paper.

Supplementary Material

SM1. *WRIID* flooding data

Support for D_R as a measure of impact comes from the Weather Related Incident Impact Data (WRIID). WRIID is Schedule 8 delay data compiled by Network Rail (NR), who are the owner and infrastructure provider of most of the rail network in Great Britain. WRIID contains 182,000 incidents (2006-2019) that have each been assigned to one of nine hazards, including flooding, and given an impact location (the originating site of delays). These data have been used previously for work on heat (83,84), linked NAO (32), and recently for multi-hazard risk (4). Precipitation data are aggregated winter England and Wales precipitation (85).

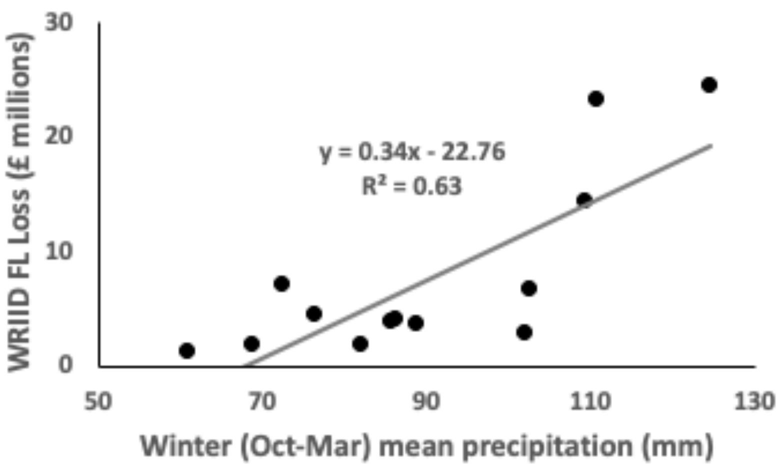

Fig. S1 - Correlation between seasonal winter flooding impacts in WRIID and monthly mean precipitation aggregated across England and Wales (85).

Pearson's correlation between seasonal winter flooding impacts in WRIID and mean monthly precipitation is r_p^2 = 0.63, with p = 0.0012, so a null hypothesis that the gradient of the line is equal to zero (2-tailed test) can be rejected. In a leave one out assessment of covariance (LOOCV) 46.4% of the variance in loss is explained by precipitation, which indicates that the relationship is not over-fitted and there is predictive capability despite the short duration of the WRIID timeseries (2006-2019). WRIID is intrinsically weighted to geographic areas with more infrastructure, but this is actually desirable in a proxy for risk.

A linear model was selected for simplicity, and to avoid overinterpreting the WRIID data. If a non-linear model is used, where the losses are related to a positive power of precipitation > 1, explanatory power is increased up to powers of 5 where r^2 = 0.78. Here, LOOCV estimates that 70.0% of the variance in losses are explained, and AIC is minimized. The model used is $y = c_1 x^n + c_2$, where c_1 and c_2 are constants, and n is a positive integer. Thus, our main results are robust to this choice, and non-parametric methods (e.g. Spearman's r) are used to verify this (e.g. Fig. S2). In future analyses, better diagnostics of impact may arise from extreme rainfall percentiles (e.g. 57) or including non-linearity before aggregation (i.e. as for D_w).

SM2. Sensitivity tests

In this approach to mapping the spatial pattern of co-occurrence of flooding and extreme wind, a number of choices were made. Fig. S2a-d demonstrates that the *relative magnitudes* of correlation at sites W (blue), E (red) and C (green) are robust to these choices; equivalent lines never cross where they are reliably constrained (site C in Fig. S2b discussed below), and whilst the use of mean uplift in U D_W as opposed to r_p or r_s raises intermediate levels of correlation (site C) to a par with higher ones (site W), but both remain distinctly above those of site E in the correlation shadow. Thus, the spatial pattern (Fig. 2d) is mainly broadly insensitive to measure of correlation used (U, r_p, r_s), threshold c selected for D_W, fraction f of years defined as 'wet' or 'dry' in order to compute U, or indeed the exact months defined as winter.

There is very little difference between Pearson's correlation coefficient (r_p) and Spearman's rank correlation (r_s), which isolates the dependency structure from the marginal distributions (Fig. S2a). This justifies the functional forms chosen such as $\log(D_W)$ for in Figs. 2a-c. A lower threshold might be argued for on the basis that SEAS5 wind speeds are averaged over a relatively large (1° x 1°) area, which would increase correlation strengths (r_p, r_s) bolstering the points in the main text. Taking a high (98th) percentile of daily max 10-m gust wind speed, which has been related to damage in UK and Germany using weather station data (34,58,86), would argue for a higher c that varies by site, but the relative magnitudes not altered by this. Fig. S2b contains the only example of relative magnitudes at sites changing, when values at site C go below those of site W or $c > 24\text{ms}^{-1}$, however this is because wind speeds are lowest at site C (Figs. 2c, S2a) and data become sparse. So, we regard this feature as unreliable. Lines are horizontal on Fig. S2c as f is not included in the computation of r_p or r_s, but it is included for completeness. Fig. S2d illustrates that, similar to Fig. S2b, mean uplift in U increases as the subset of data used is limited to include only increasingly extreme values (higher c, lower f).

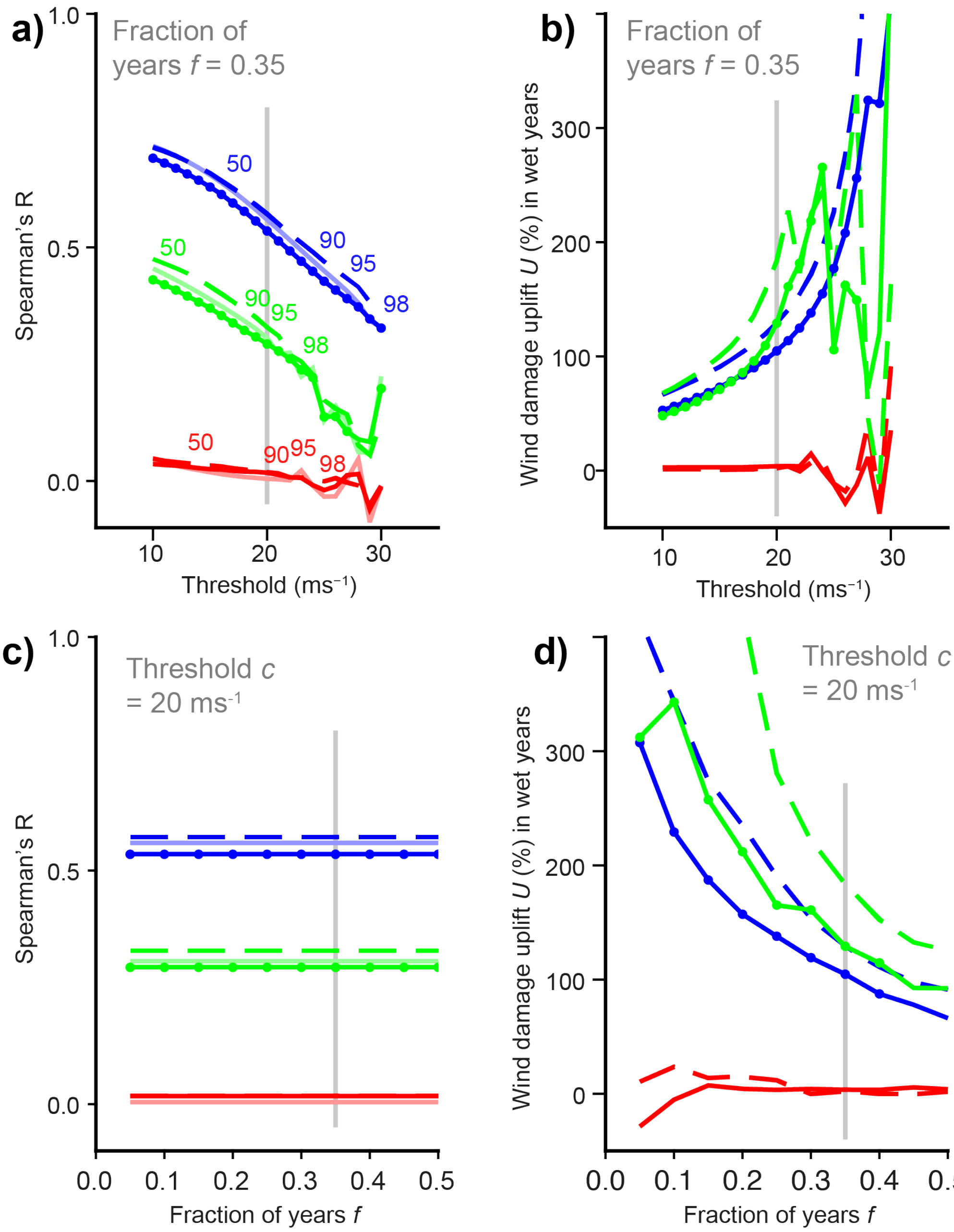

Fig. S2 - Sensitivity tests for the mapping of correlation at site W (blue), site E (red) and site C (green)**.** (a) and (b) are Spearman's rank correlation r_s, and uplift $U = 100 * (D_{w\_wet}/D_{w\_dry} - 1)$ in wet over dry years, respectively, both with the fraction (*f*) of years defined as 'wet' or 'dry' held at 0.35 whilst the threshold *c* over which v^3 is summed for D_W is varied in increments of 1 ms^{-1}. (c) and (d) are similar, except that *c* is held constant at 20ms^{-1} and *f* is varied in increments of 0.05. For these main tests only (dark solid lines) statistical significance ($p < 0.05$) is indicated by small circles, with their lack indicating insignificance. Pale solid line are for r_p instead of r_s. Dashed lines are for a shorter Nov-Feb winter. Vertical grey bars indicated the values used in Fig. 2. Percentiles of v_{max} are shown in (a) to allow comparison with percentile-based methods.

SM3. Correlations in daily data at sites W and E

To augment the main analysis using seasonal impact-based hazard proxies, daily data were examined. Figs S3 plots a selected comparison. As in the main analysis *R* is total daily precipitation in mm, v_{max} is daily max 10-m gust wind speed. Orientation is calculated from velocities to the east and north averaged over 24h, also from SEAS5. The correlation between extremes of wind and rain at site W (r_s= 0.607, Fig. S3a) is greater than that at site E (r_s= 0.069). For extremes however, within the upper-right quadrant as delimited by the dashed lines (98th percentiles), there is a notable absence of points for site W as compared to site N (Fig. S3). A simple cumulative Binomial distribution can be used to determine that there are more occurrences at site W than expected by chance (n = 109200, p = 0.02^2, *E[n]* = 43.7), in line with Martius et al. (12), but typically either wind is very extreme *or* rain is, not both (Fig. S3a,b). This supports the argument that underlying processes enduring across longer durations (>72h) are needed to generate the correlations observed (Fig. 2d).

Fig. S4 counters the idea that in the GB correlation shadows can arise from the east and west of the country experiencing different air masses (76). Orientations at the sites are similar, but with slightly more frequent winds from the south-west for site E. So, it is not possible for a difference in wind directions experienced by E can possibly explain the decorrelation between wind and rain extremes there without another factor; with all else equal, the effect of south-westerly winds driving the correlation in site W should be even more pronounced at site E. Prevailing winds from the south-west occur in historically observed 3-sec 10m gusts at a 43-station network over the period 1980–2005, with this prevalence even more pronounced for damaging winds exceeding the 98th percentile (58). So, this is not an artefact of SEAS5 at sites W and E.

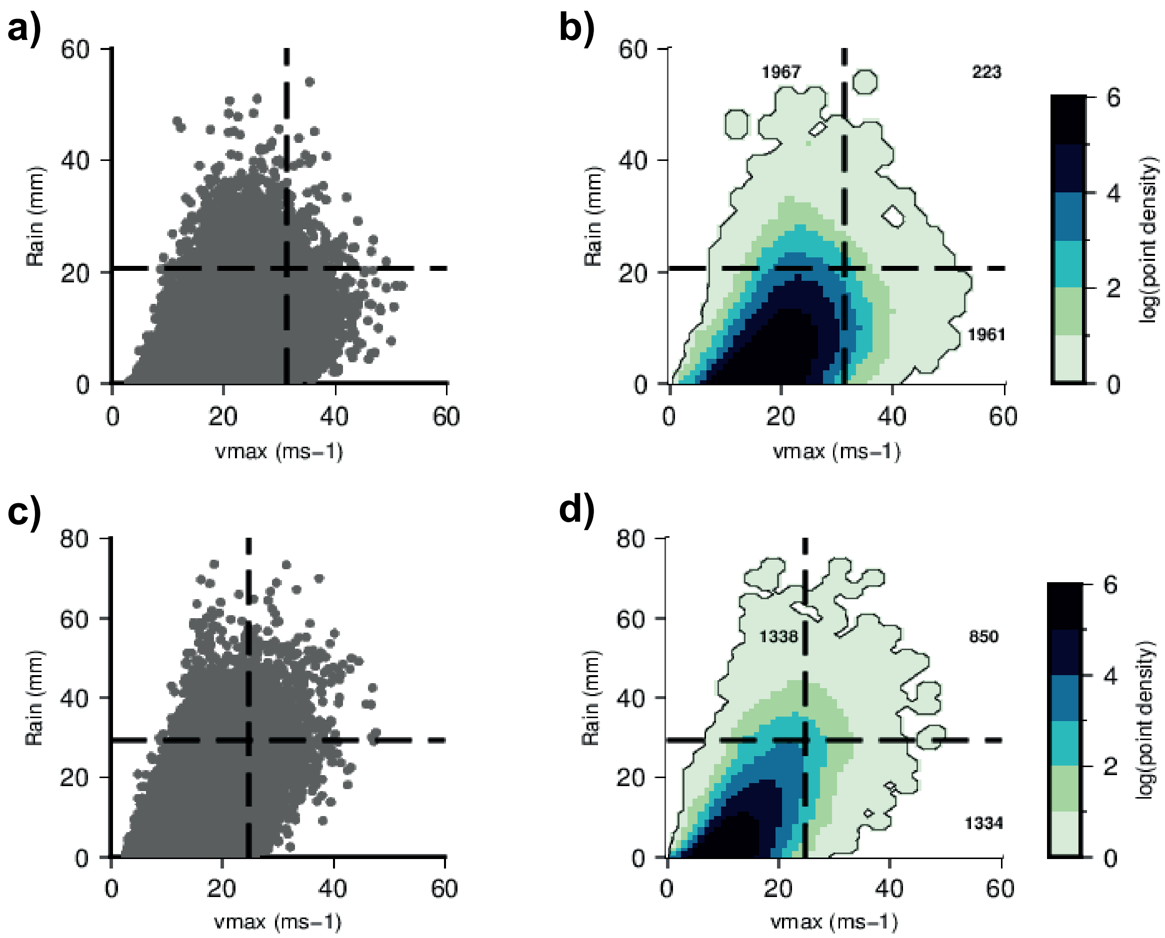

Fig. S3 - Correlation between daily *R* and v_{max} values at sites W and N. (a) All 109200 data displayed individually (grey dots) and 98th percentiles (dashed lines). (b) Structure of the point cloud for the data in panel (a), displayed as point density using a smoothing kernel of width 5 units, with dark blue shades indicating high density. Numbers in quadrants delimited by the lines are number of points in the quadrants. (c) and (d) are as for (a) and (b), but for site N.

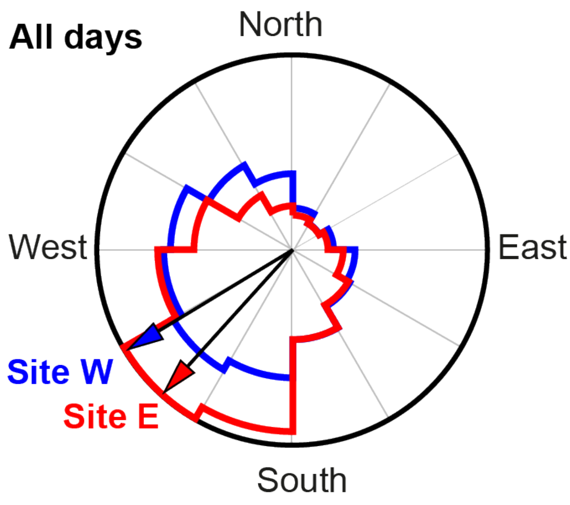

Fig. S4 - Wind direction within SEAS5. All days are used for site W (blue) and site E (red).

SM4. Trade-offs in wind direction

It is known that there is a trade-off between weather types in Great Britain (79,80). An analysis of Lamb's (1972) principal weather types (Fig. S5) confirms that previous work on these Lamb Weather Types (LWTs) applies to the trade-off most relevant to this study. The most relevant directional types here (Fig. 2e,f)(81) are northerly (N), easterly (E) and westerly (W). In Fig. S5 black dots are for the years that WRIID losses, as used in Section SM1, are available (r_p = -0.824, p = 0.0005). The red dots are for a longer period, from 1948 to 2018, and show a similar pattern (r_p = -0.725, p = ≪ 0.01).

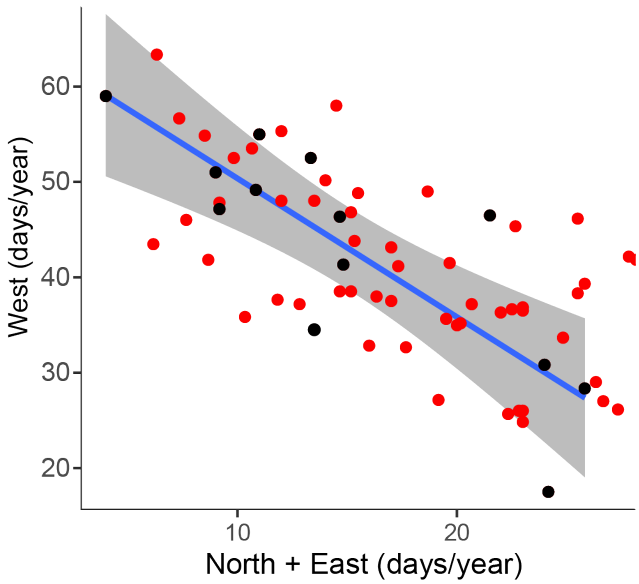

Fig. S5 - Trade-off between Lamb Weather Types for W and N&E. Black dots are for the years that WRIID losses are available (2006-2018), and red dots are for the period 1948-2018. Both show the same pattern. Data: https://crudata.uea.ac.uk/cru/data/lwt/. Trendline is for 2006-2018 data, and grey shading indicates estimated 2σ bounds for this.

SM5. Relative dominance of daily and seasonal time-scales for compounding risk

An analysis is conducted to derive a first-order indication of the relative dominances (i.e. minor, comparable, major) of short term (12) and up to seasonal (2) contributions to the compounding effect between extreme wind and a precipitation-based proxy for flooding. An approach is used in which linkages between extremes in data (e.g. SEAS5) are selectively broken to quantify the effect they had by measuring the difference their absence makes (4). For simplicity, and to isolate the correlation-related effects, flooding and wind are assumed to have the same loss distribution; this is a substantial assumption, so the detail of the results (Fig. S6) should not be over-interpreted.

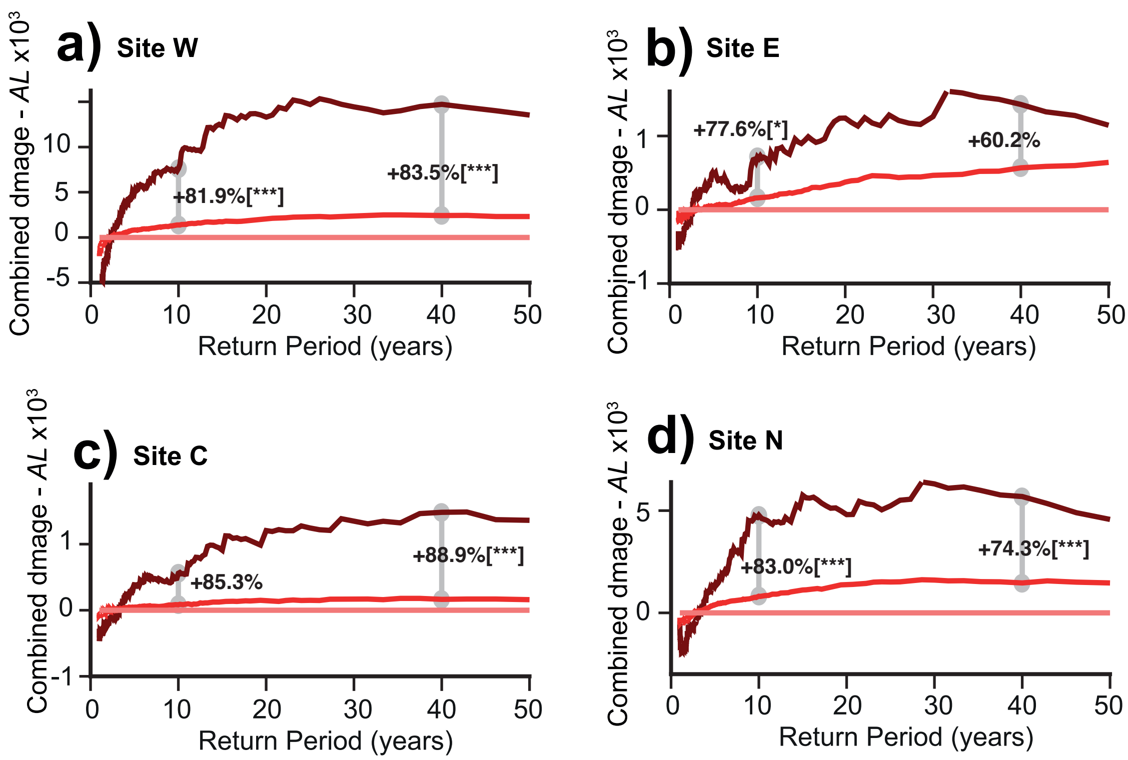

Fig. S6 - Breakdown of timescales contributing to compounding at Sites. All panels are Aggregate Exceedance Probability (AEP) plots, with a damage metric *AL* estimated for flooding and extreme wind combined displayed as a difference from a simulated condition of independence between the hazards (pink line, condition C). Data directly from SEAS5 (dark red, condition A) plot above a condition in which associations between extremes within a 72h window are retained but any longer-term relationships (e.g. monthly) are removed (red, condition B). Differences between conditions A and B, due to longer term (up to seasonal) effects, are shown at 10 and 40 year return periods (vertical grey lines). Where statistically significant, p values are in []; * <0.1, ** <0.05, *** <0.01. Total (and average) loss is identical in all 3 conditions, merely re-distributed.

Using a metric estimating flooding and extreme wind damage combined (D_W), statistical simulation modelling (Fig. S6) is conducted to provide an explanation for the increased clarity of the paired areas of enhanced-suppressed correlation in Fig. 2d. The majority (74-89%) of the compounding effect, as estimated at the 40 year return period level at key sites (W,C,N) is attributable to relationships caused by weather patterns or other climatological drivers that endure for timescales of greater than 72h. This estimate is made by taking data directly from SEAS5 (condition A), which contains all the hazard inter-dependencies within that dynamical modelling, and using simulation to break any relationship between extremes outside a ±1 day window (condition B) (12), and finally breaking relationships at all timescales (i.e. independence, condition C). Thus, A-C is the entire impact of hazard interdependency upon risk, B-C is the part attributable to short-term linkages (±1 day) (12), and A-B is the remainder due to longer term (up to seasonal) effects. The method is detailed below, sequentially for the 3 conditions.

<u>Condition A</u>

1. Extract v_{max} and *R* (1°x1°) from SEAS5 for a site, and convert the daily v_{max} winds to estimates of damage L_{wi} = {1,2,..... n} where n is the count of daily data during 600 years of October-March winters (i.e. 109200). The subscript w denotes wind. $L = (v_{max} - c)^3$ for $v_{max} > c$, taking *c* as 20 ms^{-1}, as in the main text.
2. Rank L_{wi} by magnitude.

3. Convert daily precipitation totals to estimates of damage L_{Ri} = {1,2,..... n} by ranking them according magnitude, then assigning L_{Ri} to be the L_{wi} of the same rank (i.e. extremeness according to percentile). This gives both hazards an identical, empirical marginal distribution specific to each site analysed.
4. Compute total seasonal (i.e. aggregate) losses for wind in years j = {1,2,..... n}, where n is the number of years (i.e. 600), as $AL_{jw} = \sum_i L_{iw}$ for days i within each year j. Do similar for precipitation, then add to wind losses to give combined annual losses AL_j.
5. With annual losses AL_j, calculate an AEP curve using standard methods (21) to give losses at return periods R for condition A of AL_{AR}. These form the pink line on Fig. S6.

<u>Condition B</u>

Start from Step 6. Numbering is continuous to prevent ambiguity. Note that the total value of the damage proxies in the time series remains identical

6. Perform Steps 1-5 as for Condition A, inserting the following two manipulations between steps 3 and 4. First, Identify high values of L_{wi} within a ±24h window (i.e. > at i+1 or i-1) and, for these values of i, identify the highest L_{Ri} within the ±24h window and if necessary swop it with the value at i such that the highest L_{wi} and L_{Ri} values are now coupled. Sum them (i.e. $L_i = L_{wi} + L_{Ri}$). Second, randomize i, such that losses are re-assigned to different years. Note that as damage estimates for w and R are already combined, it is not necessary to repeat this in Step 4. This creates a set of return period losses AL_{BR}.
7. Repeat Step 6 100 times to determine estimates of the mean (μ) and standard deviation (σ) of AL_{2R} for each return period R, defining Normal distributions i.e. AL_{BR} ~N(μ,σ) assuming the Central Limit Theorem applies.
8. For each return period R, calculate a two-tailed p-value using a cumulative Normal distribution that the value from Condition A (i.e. AL_{AR}) could arise from Condition B by

chance (i.e. is the difference caused by eliminating all associations outside a ±24h window statistically significant).

Condition C

Start from Step 9. Numbering is continuous to prevent ambiguity. Note that the total value of the damage proxies in the time series remains identical.

9. Perform Steps 1-5 as for Condition A, inserting the following manipulations between steps 3 and 4. For each hazard separately, randomize i such that losses are re-assigned to different years. This creates a set of return period losses AL_{CR}.
10. Repeat Step 6 100 times to determine estimates of the mean (μ) and standard deviation (σ) of AL_{CR} for each return period R, defining Normal distributions i.e. AL_{CR} ~N(μ,σ) assuming the Central Limit Theorem applies.
11. For each return period R, calculate a two-tailed p-value using a cumulative Normal distribution that the value from Condition A (i.e. AL_{1R}) could arise from Condition C by chance (i.e. is the difference caused by eliminating all associations statistically significant).

Bibliography

1. Kappes MS, Keiler M, von Elverfeldt K, Glade T. Challenges of analyzing mulit-hazard risk: a review. Nat Hazards. 2012;64:1925–1958.
2. Hillier JK, Macdonald N, Leckebusch GC, Stavrinides A. Interactions between apparently primary weather-driven hazards and their cost. Env Res Lett. 2015;10:104003.
3. de Ruiter M, Couasnon A, van den Homberg MJC, Daniell JE, Gill J, Ward PJ. Why We Can No Longer Ignore Consecutive Disasters. Earth's Future. 2019;8:e2019EF001425.
4. Hillier JK, Matthews T, Wilby RL, Murphy C. Multi-hazard dependencies can increase and decrease risk. Nature Climate Change. 2020;
5. Zscheischler J, Westra S, van der Hurk BJJM, Seneviratne SI, Ward PJ, Pitman A, et al. Future climate risk from compound events. Nature Climate Change. 2018;
6. Bevacqua E, Maraun D, Haff HI, Widmann M, Vrac M. Multivariate statistical modelling of compound events via pair-copula constructions: analysis of floods in Ravenna (Italy). Hydrol Earth Syst Sci. 2017;21:2701–23.
7. Moftakhari H, Schubert JE, AghaKouchak A, Matthew RA, Sanders, B. F. Linking statistical and hydrodynamic modeling for compound flood hazard assessment in tidal channels and estuaries. Advances in Water Resources. 2019;128:28–38.
8. Khouakhi A, Villarini G. Contribution of tropical cyclones to rainfall at global scale. Journal of Climate. 2017;30:359–372.
9. Matthews T, Wilby RL, Murphy C. An emerging tropical cyclone–deadly heat compound hazard. Nature Climate Change. 2019;9:602–6.
10. Ward PJ, Couasnon A, Eilander D, Haigh ID, Hendry A, Muis S, et al. Dependence between high sea-level and high river discharge increases flood hazard in global deltas and estuaries. Env Res Lett. 2018;13(8):084012.
11. De Luca P, Hillier JK, Wilby RL, Quinn NW, Harrigan S. Extreme multi-basin flooding linked with extra-tropical cyclones. Env Res Lett. 2017;12(11):114009.
12. Martius O, Pfahl S, Chevalier C. A global quantification of compound precipitation and wind extremes: Compound precipitation and wind extremes. Geophys Res Lett. 2016;43:7709–14.
13. Steptoe H, Jones SEO, Fox H. Correlations between extreme atmospheric hazards and global teleconnections: Implications for multi-hazard resilience. Reviews of Geophysics. 2017;55(1):50–78.
14. Walz MA, Donat MG, Leckebusch GC. Large-Scale Drivers and Seasonal Predictability of Extreme Wind Speeds Over the North Atlantic and Europe. Journal of Geophysical Research: Atmospheres. 2018;123(20):11518–35.
15. Chan JCL. Interannual variations of intense typhoon activity. Tellus, Series A: Dynamic Meteorology and Oceanography. 2007;59(A(4)):455–460.
16. Camargo SJ, Sobel AH. Western North Pacific Tropical Cyclone Intensity and ENSO. Journal of Climate. 2010;23:5810–5825.

17. Mariani M, Fletcher MS, Holz A, Nyman P. ENSO controls interannual fire activity in southeast Australia. Geophys Res Lett. 2016;43:10891–900.

18. Bieli M, Pfahl S, Wernli H. A Lagrangian investigation of hot and cold temperature extremes in Europe. Quaterly Journal of the Royal Meteorological Society. 2015;141:98–108.

19. West H, Quinn N, Horswell M. Regional Rainfall Response to the North Atlantic Oscillation (NAO) across Great Britain. Hydrology Research. 2019;50(6):1549–63.

20. Zscheischler J, Seneviratne SI. Dependence of drivers affects risks associated with compound events. Science Advances. 2017;3:e1700263.

21. Mitchell-Wallace K, Jones M, Hillier JK, Foote M. Natural Catastrophe Risk Management and Modelling: A Practitioner's Guide. Oxford, UK: Wiley; 2017. 506 p.

22. Donat MG, Leckebusch GC, Wild S, Ulbrich U. Future changes in European winter storm losses and extreme wind speeds inferred from GCM and RCM multi-model simulations. Nat Hazards Earth Syst Sci. 2011;11:1351–1370.

23. Lavers DA, Allan RP, Villarini G, Lloyd-Hughes B, Brayshaw DJ, Wade AJ. Future changes in atmospheric rivers and their implications for winter flooding in Britain. Environmental Research Letters. 2013;8(3):034010.

24. Matthews T, Murphy C, McCarthy G, Broderik C, Wilby RL. Super Storm Desmond: a process-based assessment. Env Res Lett. 2018;13(1):014024.

25. Otto F, van der Wiel K, van Oldenborgh GJ. Climate change increases the probability of heavy rains in Northern England/Southern Scotland like those of storm Desmond-a real-time event attribution revisited. Environmental Research Letters. 2018;13(2):024006.

26. Fink AH, Brucher T, Ermert V, Kruger A, Pinto JG. The European storm Kyrill in January 2007: Synoptic evolution, meteorological impacts and some considerations with respect to climate change. Nat Hazards Earth Syst Sci. 2009;9:405–23.

27. Raveh-Rubin. Large-scale wind and precipitation extremes in the Mediterranean: A climatological analysis for 1979–2012. Q J R Meteorol Soc. 2015;141:2404–17.

28. Liberato MLR. The 19 January 2013 windstorm over the North Atlantic: Large-scale dynamics and impacts on Iberia. Weather Clim Extremes. 2014;5–6:16–28.

29. Matthews T, Murphy C, Wilby RL, Harrigan S. Stormiest winter on record for Ireland and UK. Nature Climate Change. 2014;4:738–740.

30. De Luca P, Messori G, Pons FME, Faranda D. Dynamical systems theory sheds new light on compound climate extremes in Europe and Eastern North America. Quart J Royal Meteorol Soc. 2020;

31. Zscheischler J, Mahecha MD, von Buttlar J, Harmeling S, Jung M, Rammig A, et al. A few extreme events dominate global interannual variability in gross primary production. Env Res Lett. 2014;9:035001.

32. Palin EJ, Scaife AA, Wallace E, Pope E, Arribas A, Brookshaw A. Skillful Seasonal Forecasts of Winter Disruption to the U.K. Transport System. Journal of Applied Meteorology and Climatology. 2016;55:325–44.

33. Emanuel K. Increasing destructiveness of tropical cyclones overthe past 30 years. Nature. 2005;436:686–8.

34. Klawa M, Ulbrich U. A model for the estimation of storm losses and the identification of severe winter storms in Germany. Nat Hazards Earth Syst Sci. 2003;3(6):725–32.

35. Geiger T, Frieler K, Bresch D. A global historical data set of tropical cyclone exposure (TCE-DAT). Earth System Science Data. 2013;10:185–194.

36. Hawker M. Climate Change and the Global Insurance Industry. The Geneva Papers. 2007;32:22–8.

37. Nordhaus W. The economics of hurricanes and implications of global warming. Climate Change Economics. 2010;1(1–20).

38. Southern RL. The global socio-economic impact of tropical cyclones. Aust MeteorolMag. 1979;27:175–95.

39. Postance B, Hillier JK, Dijkstra T, Dixon N. Comparing threshold definition techniques for rainfall-induced landslides: A national assessment using radar rainfall. Earth Surface Processes and Landforms. 2017;43(2):553–60.

40. Berghuijs WR, Harrigan S, Molnar P, Slater L, Kirchner JW. The relative importance of different flood-generating mechanisms across Europe. Water Resour Res. 2019;55(6):4582–93.

41. Johnson SJ, Stockdale T, Ferranti L, Balmaseda M, Molteni F, Magnusson L, et al. SEAS5: the new ECMWF seasonal forecast system. Geosci Model Dev. 2019;12:1087–117.

42. CDS. CDS Home Page. 2020 [cited 2020 Apr 30]. Available from: https://cds.climate.copernicus.eu/#!/home

43. Osinski R, Lorenz P, Kruschke T, Voigt M, Ulbrich U, Leckebusch GC, et al. An approach to build an event set of European wind storms based on ECMWF EPS. Nat Hazards Earth Syst Sci Discuss. 2016;16(1):255–68.

44. Walz MA, Leckebusch GC. Loss potentials based on an ensemble forecast: How likely are winter windstorm losses similar to 1990? Atmospheric Science Letters. 2019;

45. Stockdale T, Johnson S, Ferranti L, Balmaseda M, Briceag S. ECMWF's new long-range forecasting system SEAS5. ECMWF Newsletter [Internet]. 2018 [cited 2020 Feb 12];154. Available from: https://www.ecmwf.int/en/newsletter/154/meteorology/ecmwfs-new-long-range-forecasting-system-seas5

46. van den Brink HW, Können GP, Opsteegh JD, van Oldenborgh GJ, Burgers G. Improving 10^4-year surge level estimates using data of the ECMWF seasonal prediction system. Geophys Res Lett. 2004;31:L17210.

47. Breivik Ø, Aarnes OJ, Abadalla S, Bidlot J-R, Janssen P. Wind and Wave Extremes over the World Oceans From Very Large Ensembles. Geophys Res Lett. 2014;41:5122–5131.

48. Thompson V, Dunstone NJ, Scaife AA, Smith DM, Slingo JM, Brown S, et al. High risk of unprecedented UK rainfall in the current climate. Nature communications. 2017;8(1):107.

49. Kelder T, Muller M, Slater L, Marjoribanks T, Wilby RL, Prudhomme C, et al. UNSEEN trends: Detecting decadal changes in 100-year precipitation extremes. In Prep.; Available from: https://eartharxiv.org/hyxeq/

50. Muir-Wood R, Drayton M, Berger A, Burgess P, Wright T. Catastrophe loss modelling of storm-surge flood risk in eastern England. Phil Trans Royal Soc London A. 2005;1407–22.

51. Lamb R, Keef C, Tawn J, Laeger S, Meadowcroft I, Surendran S, et al. A new method to assess the risk of local and widespread £ooding on rivers and coasts. Journal of Flood Risk Management. 2010;3:323–36.

52. Wyncoll D, Gouldby B. Integrating a multivariate extreme value method within a system flood risk analysis. Journal of Flood Risk Management. 2013;8(2):145–160.

53. Serinaldi F, Papalexiou SM. Random fields simplified: Preserving marginal distributions, correlations, and intermittency, with applications from rainfall to humidity. Water Resour Res. 2020;56(2):e2019WR026331.

54. Wadsworth JL, Tawn JA, Davidson AC, Elton DM. Modelling across extremal dependence classes. Journal Of The Royal Statistical Society Series B. 2017;79(1):149–75.

55. Hao Z, Hao F, Singh VP, Xia Y, Shi C, Zhang X. A multivariate approach for statistical assessments of compound extremes. Journal of Hydrology. 2018;565:87–94.

56. Hao Z, Singh VP, Hao F. Compound Extremes in Hydroclimatology: A Review. Water. 2018;10(6):art. no. 718.

57. Malby AR, Whyatt JD, Timmis RJ, Wilby RL, Orr HG. Long-term variations in orographic rainfall: analysis and implications for upland catchments. Hydrological Sciences. 2007;52(2):276–91.

58. Hewston R, Dorling SR. An analysis of observed daily maximum wind gusts in the UK. Journal of Wind Engineering and Industrial Aerodynamics. 2011;99:845–56.

59. Douglas CKM, Glasspoole J. Meteorological conditions in heavy orographic rainfall. Quart J Royal Meteorol Soc. 1947;73:11–38.

60. Hill FF, Browning KA, Bader MJ. Radar and rain gauge observations of orographic rain over south Wales. 1981;107:643–70.

61. Smith SA, Vosper SB, Field PR. Sensitivity of orographic precipitation enhancement to horizontal resolution in the operational Met Office Weather forecasts. Meteorological Applications. 2012;22:14–24.

62. Bergeron T. On the low-level redistribution of atmospheric water caused by orography. In: Supplementary Proceedings of the International Conference on Cloud Physics. Tokyo, Japan.: IAMAP/WMO; 1965. p. 96–100.

63. Dore AJ, Choularton TW, Brown R, Blackall RM. Orographic rainfall enhancement in the mountains of the Lake District and Snowdonia. Atmospheric Environment. 1992;26A(3):357–71.

64. Sibley A, Cox D, Titley H. Coastal flooding in England and Wales from Atlantic and North Sea storms during the 2013/2014 winter. Weather. 2015;70(2):62–70.

65. Eden P, Burt S. Extreme rainfall in Cumbria, 18–20 November 2009. Weather. 2010;65(1):14.

66. Roberts NM, Cole SJ, Forbes RM, Moore RJ, Boswell D. Use of high-resolution NWP rainfall and river flow forecasts for advance warning of the Carlisle flood, north-west England. Meteorological Applications. 2009;16:23–34.

67. Geng Q, Sugi M. Variability of the North Atlantic Cyclone Activity in Winter Analyzed from NCEP–NCAR Reanalysis Data. Journal of Climate. 2001;14:3863–73.

68. Ulbrich U, Leckebusch GC, Pinto JG. Extra-tropical cyclones in the present and future climate: a review. Theor Appl Climatol. 2009;96:117–31.

69. Loridan T, Scherer E, Dixon M, Bellone E, Khare S. Cyclone Wind Field Asymmetries during Extratropical Transition in the Western North Pacific. Journal of Applied Meteorology and Climatology. 2014;53:421–8.

70. Vitolo R, Stephenson DS, Cook I, Mitchell-Wallace K. Serial clustering of intense European storms. Meteorologische Zeitschrift. 2009;18(4):411–424.

71. Kendon M, McCarthy M. The UK's wet and stormy winter of 2013/2014. Weather. 2015;7(2):40–47.

72. Huntingford C, Marsh T, Scaife AA, Kendon EJ. Potential influences on the United Kingdom's floods of winter 2013/14. Nature Climate Change. 2014;4:769–777.

73. Wild S, Befort DJ, Leckebusch GC. Was the extreme storm season 2013-14 over the North Atlantic and the UK triggered by changes in the West-Pacific Warm Pool? Bulletin of the American Meteorological Society. 2015;

74. Smith RB. The influence of mountains on the atmosphere. Advances in Geophysics. 1979;21:87–230.

75. Sinclair MR. A diagnostic model for estimating orographic precipitation. Journal of Applied Meteorology. 1994;33:1163–75.

76. Stockham AJ, Schultz DM, Fairman JG, Draude AP. Quantifying the rain-shadow effect: Results from the Peak District, British Isles. Bulletin of the American Meteorological Society. 2018;778–90.

77. Silner N, Roe G, Durran D. On the dynamical causes of variability in the rain-shadow effect: A case study of the Washington Cascades. Journal of Hydrometeorology. 2013;14:122–39.

78. Mass C, Johnson N, Warner N, Vargas R. Synoptic control of cross-barrier precipitation ratios for the Cascade Mountains. Journal of Hydrometeorology. 2015;16:1014–28.

79. Briffa KR, Jones PD, Kelly PM. Principal component analysis of the Lamb catalogue of daily weather types: Part 2, Seasonal frequencies and update to 1987. International Journal of Climatology. 1990;10(6):549–63.

80. Jones PD, Osborn TJ, Harpham C, Briffa KR. The Development of Lamb Weather types: from subjective analysis of weather charts to objective approaches using Reanalyses. Weather. 2014;69(5):128–32.

81. Wilby RL, Quinn NW. Reconstructing multi-decadal variations in fluvial flood risk using atmospheric circulation patterns. Journal of Hydrology. 2013;487:109–121.

82. Halliday O, Shafferty L, Tsaknias D, Siddaway A, Cloke H. Understanding the Risk from Correlated Windstorms and Floods in the UK. In Prep.; Available from: https://presentations.copernicus.org/EGU2020/EGU2020-20230_presentation.pdf

83. Ferranti EJS, Chapman L, Lowe C, McCulloch S, Jaroszweski D, Quinn AD. Heat-related failures on South-East England's railway network: insights and implications for heat-risk management. Weather Climate and Society. 2016;8:177–91.

84. Ferranti EJS, Jaroszweski D, Lee S, Chapman L, Lowe C, Quinn AD. The hottest day on the railway network; insights and thoughts for the future. Meteorological Applications. 2018;5:195–208.

85. HadUKP. 2019. Available from: https://www.metoffice.gov.uk/hadobs/hadukp/data/download.html

86. Hewston R. Quantifying the Impact of Historical and Future Climate Change on Windstorm Insured Loss in Great Britain [PhD]. [Norwich]: School of Environmental Sciences, University of East Anglia; 2008.